

Cutoff effects on energy-momentum tensor correlators in lattice gauge theory

Harvey B. Meyer

*Center for Theoretical Physics
Massachusetts Institute of Technology
Cambridge, MA 02139, U.S.A.
E-mail: meyerh@mit.edu*

ABSTRACT: We investigate the discretization errors affecting correlators of the energy-momentum tensor $T_{\mu\nu}$ at finite temperature in $SU(N_c)$ gauge theory with the Wilson action and two different discretizations of $T_{\mu\nu}$. We do so by using lattice perturbation theory and non-perturbative Monte-Carlo simulations. These correlators, which are functions of Euclidean time x_0 and spatial momentum \mathbf{p} , are the starting point for a lattice study of the transport properties of the gluon plasma. We find that the correlator of the energy $\int d^3x T_{00}$ has much larger discretization errors than the correlator of momentum $\int d^3x T_{0k}$. Secondly, the shear and diagonal stress correlators (T_{12} and T_{kk}) require $N_\tau \geq 8$ for the $Tx_0 = \frac{1}{2}$ point to be in the scaling region and the cutoff effect to be less than 10%. We then show that their discretization errors on an anisotropic lattice with $a_\sigma/a_\tau = 2$ are comparable to those on the isotropic lattice with the same temporal lattice spacing. Finally, we also study finite \mathbf{p} correlators.

KEYWORDS: Lattice QCD, Thermal Field Theory.

Contents

1. Introduction	1
2. Definitions and master formulas	2
2.1 In the continuum	2
2.2 On the lattice	2
2.3 Clover discretization	3
2.4 Plaquette discretization	4
3. Investigating cutoff effects	5
3.1 Correlators of conserved charges	5
3.2 The tensor channel ($\xi = 1$)	5
3.3 The scalar channel ($\xi = 1$)	6
3.3.1 Asymptotic temperatures	6
3.3.2 Temperatures close to T_c	7
3.4 Anisotropic lattice	7
3.5 Non-zero spatial momentum	7
4. Treelevel improvement	7
5. Non-perturbative study of cutoff effects	8
5.1 Isotropic lattice, plaquette discretization	8
5.2 Anisotropic lattice ($\xi = 2$), clover discretization	8
6. Concluding remarks	8

1. Introduction

Energy-momentum tensor (EMT) correlators in finite-temperature QCD provide a way to study the spatial correlation of fluctuations in energy density, pressure and entropy [1]. They thus allow us to gain insight into the structure of the quark-gluon plasma (QGP), thereby going beyond its thermodynamic properties. The time-dependent EMT correlators are related to the transport properties of the QGP. Phenomenological upper bounds for the shear viscosity to entropy density ratio, $\eta/s < \frac{5}{4\pi}$ (see [2] and Refs. therein), are derived by comparing hydrodynamic calculations of elliptic flow to heavy ion collision data. This result suggests the picture of a strongly coupled plasma around $2T_c$, where T_c is the QCD crossover temperature. A significant effort is underway to constrain the transport properties of the gluonic sector non-perturbatively from first principles [3, 4], and given the high computational cost of determining the EMT correlators in Monte-Carlo simulations, it is important to optimize the choice of lattice action and discretization of the EMT. This is the subject of this paper.

The gluonic correlators have been computed at treelevel in the continuum [5]. Here we compute the correlators at finite lattice spacing using the (anisotropic) Wilson plaquette action [6] and two

discretizations of the EMT. The strategy is to determine the kinematic regime where the treelevel discretization errors are below the 10% level. We then expect treelevel improvement to further reduce the discretization errors to the few percent level. This is a reasonable target, given the statistical accuracy being currently achieved in lattice simulations [4].

The outline of this paper is as follows. In section 2 we give the definitions of the lattice actions and discretizations of the EMT, and derive the treelevel formulas for the two-point functions on the lattice. Section 3 is devoted to analyzing the treelevel cutoff effects for various correlators. Section 4 describes how the treelevel discretization errors can be removed from non-perturbative Monte-Carlo data, and in section 5 we discuss to what extent treelevel improvement is successful. We end with some concluding remarks.

2. Definitions and master formulas

2.1 In the continuum

The continuum Euclidean energy-momentum tensor for $SU(N_c)$ gauge theories reads

$$T_{\mu\nu}(x) = \theta_{\mu\nu}(x) + \frac{1}{4}\delta_{\mu\nu}\theta(x) \quad (2.1)$$

$$\theta_{\mu\nu}(x) = \frac{1}{4}\delta_{\mu\nu}F_{\rho\sigma}^a F_{\rho\sigma}^a - F_{\mu\alpha}^a F_{\nu\alpha}^a \quad (2.2)$$

$$\theta(x) = \frac{\beta(g)}{2g} F_{\rho\sigma}^a F_{\rho\sigma}^a \quad (2.3)$$

$$\beta(g) = -b_0 g^3 + \dots, \quad b_0 = \frac{11N_c}{3(4\pi)^2}. \quad (2.4)$$

We will study the dimensionless, finite-temperature T Euclidean correlators

$$C_{\mu\nu,\rho\sigma}(x_0, \mathbf{p}) \equiv T^{-5} \int d^3\mathbf{x} e^{i\mathbf{p}\cdot\mathbf{x}} \langle T_{\mu\nu}(x_0, \mathbf{x}) T_{\rho\sigma}(0) \rangle. \quad (2.5)$$

$C_{\mu\nu,\mu\nu}$ (no summation) will be sometimes abbreviated as $C_{\mu\nu}$, and $C_{\theta\theta}$ is the correlator of the trace anomaly θ , normalized as in Eq. (2.5). In the continuum, these correlators were calculated to leading order in perturbation theory in [5]. The extent of the time direction is denoted by $L_0 \equiv 1/T$.

2.2 On the lattice

On the anisotropic lattice with spatial lattice spacing a_σ and temporal lattice spacing a_τ , the Wilson action reads

$$S_g = \sum_x \beta_\sigma S_\sigma(x) + \beta_\tau S_\tau(x). \quad (2.6)$$

In numerical practice, it is convenient to parametrize these parameters as

$$\beta_\sigma = \frac{\beta}{\xi_0} \quad \beta_\tau = \beta\xi_0. \quad (2.7)$$

At treelevel, $\xi_0 = a_\sigma/a_\tau$. We use the notation

$$S_\sigma = \sum_{k<l} S_{kl}, \quad S_\tau = \sum_k S_{0k}, \quad S_{\mu\nu}(x) = \frac{1}{N_c} \text{Re Tr} \{1 - P_{\mu\nu}(x)\}, \quad (2.8)$$

$$P_{\mu\nu}(x) = U_\mu(x)U_\nu(x + a_\mu\hat{\mu})U_\mu(x + a_\nu\hat{\nu})^{-1}U_\nu(x)^{-1}. \quad (2.9)$$

The lattice spacing in the four directions are denoted by a_μ in order to maintain the symmetry among different directions as long as possible. At the end of the calculation we will set $a_1 = a_2 =$

$a_3 = a_\sigma$ and $a_0 = a_\tau$. The vectors $\hat{\mu}$ are defined as unit vectors along the lattice axes. We employ the summation convention for color indices, but not for space-time indices. We use the standard notations

$$\partial_\mu f(x) = \frac{1}{a_\mu} (f(x + a_\mu \hat{\mu}) - f(x)), \quad \partial_\mu^* f(x) = \frac{1}{a_\mu} (f(x) - f(x - a_\mu \hat{\mu})), \quad \tilde{\partial}_\mu = \frac{1}{2} (\partial_\mu + \partial_\mu^*), \quad (2.10)$$

$$\hat{p}_\mu = \frac{2}{a_\mu} \sin \frac{a_\mu p_\mu}{2}, \quad \dot{p}_\mu = \frac{1}{a_\mu} \sin a_\mu p_\mu, \quad \hat{p}^2 = \sum_{\mu=0}^3 \hat{p}_\mu^2. \quad (2.11)$$

We introduce the perturbative fields $A_\mu(x)$ by

$$U_\mu(x) = e^{g_0 a_\mu A_\mu(x)}. \quad (2.12)$$

Using an antihermitian set of generators normalized by $\text{Tr} \{T^a T^b\} = -\frac{\delta_{ab}}{2}$, we define $A_\mu(x) = A_\mu^a(x) T^a$. The latter has the covariant-gauge propagator

$$\langle A_\mu^a(x) A_\nu^b(y) \rangle_0 = \delta^{ab} \int_{\mathcal{B}} \frac{d^4 p}{(2\pi)^4} \frac{e^{i(p(x-y) + \frac{1}{2} a_\mu p_\mu - \frac{1}{2} a_\nu p_\nu)}}{\hat{p}^2} \left\{ \delta_{\mu\nu} - (1 - \lambda_0^{-1}) \frac{\hat{p}_\mu \hat{p}_\nu}{\hat{p}^2} \right\}. \quad (2.13)$$

The expectation value $\langle \dots \rangle_0$ is taken in the free theory. Here and in the following, $\langle O_1 O_2 \rangle$ (whether in the free theory or not) will always be understood to be the connected two-point function. The Brillouin zone is $\mathcal{B} = \otimes_\mu \mathcal{B}_\mu$ with $\mathcal{B}_\mu = [-\pi/a_\mu, \pi/a_\mu]$. The lattice field strength is defined by

$$P_{\mu\nu}(x) \equiv \exp\{g_0 a_\mu a_\nu F_{\mu\nu}(x)\}. \quad (2.14)$$

To leading order, one has

$$F_{\mu\nu}(x) = \partial_\mu A_\nu(x) - \partial_\nu A_\mu(x) + \mathcal{O}(g_0). \quad (2.15)$$

2.3 Clover discretization

We introduce $Q_{\mu\nu}(x)$ and $\hat{F}_{\mu\nu}(x)$ as in [7],

$$Q_{\mu\nu}(x) = P_{\mu\nu}(x) + P_{\mu\nu}(x - a_\mu \hat{\mu}) + P_{\mu\nu}(x - a_\nu \hat{\nu}) + P_{\mu\nu}(x - a_\mu \hat{\mu} - a_\nu \hat{\nu}), \quad (2.16)$$

$$\hat{F}_{\mu\nu}(x) = \frac{1}{8a_\mu a_\nu} (Q_{\mu\nu}(x) - Q_{\nu\mu}(x)). \quad (2.17)$$

We define $\hat{F}_{\mu\nu}^a = g_0 \hat{F}_{\mu\nu}^a T^a$, implying for instance $-\frac{2}{g_0^2} \text{Tr} \{ \hat{F}_{\mu\nu}(x) \hat{F}_{\mu\nu}(x) \} = \hat{F}_{\mu\nu}^a(x) \hat{F}_{\mu\nu}^a(x)$. Then

$$\hat{F}_{\mu\nu}^a(x) = \frac{1}{2} \left[\tilde{\partial}_\mu (A_\nu^a(x) + A_\nu^a(x - \hat{\nu})) - \tilde{\partial}_\nu (A_\mu^a(x) + A_\mu^a(x - \hat{\mu})) + \mathcal{O}(g_0) \right].$$

Using Wick's theorem, one finds¹ ($d_A = N_c^2 - 1$)

$$\begin{aligned} & \langle \hat{F}_{\mu\nu}^a(x) \hat{F}_{\rho\sigma}^a(x) \hat{F}_{\alpha\beta}^b(y) \hat{F}_{\gamma\delta}^b(y) \rangle_0 \\ &= d_A \left[\langle \hat{F}_{\mu\nu}(x) \hat{F}_{\alpha\beta}(y) \rangle_0 \langle \hat{F}_{\rho\sigma}(x) \hat{F}_{\gamma\delta}(y) \rangle_0 + \langle \hat{F}_{\mu\nu}(x) \hat{F}_{\gamma\delta}(y) \rangle_0 \langle \hat{F}_{\rho\sigma}(x) \hat{F}_{\alpha\beta}(y) \rangle_0 \right] \Big|_{\text{U}(1)}. \end{aligned}$$

¹If O_i^a are linear combinations of the gauge fields, $O_i^a = \lambda_{i,\alpha} A_\alpha^a$, then by Wick's theorem

$$\begin{aligned} \sum_{a,b} \langle (O_1^a O_2^a) (O_3^b O_4^b) \rangle_{0,\text{conn}} &= \sum_a \langle O_1^a O_3^a \rangle_0 \langle O_2^a O_4^a \rangle_0 + \langle O_1^a O_4^a \rangle_0 \langle O_2^a O_3^a \rangle_0 \\ &= d_A (\langle O_1 O_3 \rangle \langle O_2 O_4 \rangle + \langle O_1 O_4 \rangle \langle O_2 O_3 \rangle) \Big|_{\text{U}(1)}. \end{aligned}$$

The second equality follows from the fact that $\langle O_1^a O_2^a \rangle_0$ is independent of a and equal to the corresponding correlation function in the U(1) gauge theory.

Then, in Feynman gauge $\lambda_0 = 1$, we obtain

$$\langle \widehat{F}_{\mu\nu}(x) \widehat{F}_{\alpha\beta}(y) \rangle = d_A \phi_{\mu\nu\alpha\beta}(x-y), \quad (2.18)$$

$$\phi_{\mu\nu\alpha\beta}(x) \equiv \delta_{\nu\beta} f_{\mu\alpha}^\nu(x) + \delta_{\mu\alpha} f_{\nu\beta}^\mu(x) - \delta_{\mu\beta} f_{\nu\alpha}^\mu(x) - \delta_{\nu\alpha} f_{\mu\beta}^\nu(x), \quad (2.19)$$

$$f_{\mu\alpha}^\nu(x) \equiv \int_{\mathcal{B}} \frac{d^4 p}{(2\pi)^4} \frac{e^{ipx}}{\hat{p}^2} \cos^2(p_\nu a_\nu / 2) \dot{p}_\alpha \dot{p}_\mu. \quad (2.20)$$

Finally,

$$\langle \widehat{F}_{\mu\nu}^a(x) \widehat{F}_{\rho\sigma}^a(x) \widehat{F}_{\alpha\beta}^b(y) \widehat{F}_{\gamma\delta}^b(y) \rangle_0 = d_A \left[\phi_{\mu\nu\alpha\beta}(x-y) \phi_{\rho\sigma\gamma\delta}(x-y) + \phi_{\mu\nu\gamma\delta}(x-y) \phi_{\rho\sigma\alpha\beta}(x-y) \right]. \quad (2.21)$$

This correlator is gauge-invariant and therefore independent of λ_0 . To go over to mixed propagators (which are functions of (x_0, \mathbf{p})), we introduce the spatial Fourier transform of $\phi_{\mu\nu\alpha\beta}(x)$, $\tilde{\phi}_{\mu\nu\alpha\beta}(x_0, \mathbf{p}) = a_\sigma^3 \sum_{\mathbf{x}} \phi_{\mu\nu\alpha\beta}(x) e^{i\mathbf{p}\cdot\mathbf{x}}$. Then

$$\begin{aligned} & a_\sigma^3 \sum_{\mathbf{y}} e^{i\mathbf{q}\cdot\mathbf{y}} \langle \widehat{F}_{\mu\nu}^a(0) \widehat{F}_{\rho\sigma}^a(0) \widehat{F}_{\alpha\beta}^b(x_0, \mathbf{y}) \widehat{F}_{\gamma\delta}^b(x_0, \mathbf{y}) \rangle_0 \\ &= d_A \int_{\mathcal{B}_\sigma} \frac{d^3 \mathbf{p}}{(2\pi)^3} \left[\tilde{\phi}_{\mu\nu\alpha\beta}(x_0, \mathbf{p}) \tilde{\phi}_{\rho\sigma\gamma\delta}(x_0, -(\mathbf{p} + \mathbf{q})) + \tilde{\phi}_{\mu\nu\gamma\delta}(x_0, \mathbf{p}) \tilde{\phi}_{\rho\sigma\alpha\beta}(x_0, -(\mathbf{p} + \mathbf{q})) \right]. \end{aligned} \quad (2.22)$$

with $\mathcal{B}_\sigma = \mathcal{B}_1 \times \mathcal{B}_2 \times \mathcal{B}_3$. Eq. (2.22) is the master formula from which we will derive all results in section 2.

Explicitly, in the clover case,

$$\begin{aligned} \tilde{\phi}_{\mu\nu\alpha\beta}(x_0, \mathbf{p}) &= \int_{\mathcal{B}_0} \frac{dp_0}{2\pi} \frac{e^{ip_0 x_0}}{\hat{p}_0^2 + \hat{\mathbf{p}}^2} \times \\ &\times \left[\delta_{\nu\beta} \cos^2(a_\nu p_\nu / 2) \dot{p}_\mu \dot{p}_\alpha + \delta_{\mu\alpha} \cos^2(a_\mu p_\mu / 2) \dot{p}_\nu \dot{p}_\beta \right. \\ &\quad \left. - \delta_{\mu\beta} \cos^2(a_\mu p_\mu / 2) \dot{p}_\nu \dot{p}_\alpha - \delta_{\nu\alpha} \cos^2(a_\nu p_\nu / 2) \dot{p}_\mu \dot{p}_\beta \right]. \end{aligned} \quad (2.23)$$

At finite temperature, one is to replace the p_0 -integral in $\tilde{\phi}$ by a Matsubara sum,

$$\int_{\mathcal{B}_0} \frac{dp_0}{2\pi} \rightarrow T \sum_{p_0 \in \mathcal{B}_0}, \quad p_0 = 2\pi nT, \quad n \in \mathbf{Z}. \quad (2.24)$$

It is worth noting that the scalar propagator in the mixed (x_0, \mathbf{p}) representation can be calculated explicitly, even at finite lattice spacing [8]:

$$\frac{1}{L_0} \sum_{p_0 \in \mathcal{B}_0} \frac{e^{ip_0 x_0}}{\hat{p}_0^2 + \omega^2} = \frac{a_\tau}{2} \frac{\cosh(\hat{\omega}(\frac{1}{2}L_0 - x_0))}{\sinh(\hat{\omega}a_\tau) \sinh(\frac{1}{2}\hat{\omega}L_0)}, \quad \frac{2}{a_\tau} \sinh\left(\frac{\hat{\omega}a_\tau}{2}\right) = \omega. \quad (2.25)$$

2.4 Plaquette discretization

The gauge-invariant continuum operator $[F_{\mu\nu}^a(x) F_{\mu\nu}^a(x)]_{\text{cont}}$ can be discretized gauge invariantly as

$$\frac{4}{g_0^2 a_\mu^2 a_\nu^2} \text{Re Tr} \{1 - P_{\mu\nu}(x)\} = F_{\mu\nu}^a(x) F_{\mu\nu}^a(x) + \mathcal{O}(a_{\mu,\nu}^2), \quad (2.26)$$

by the lattice field $F_{\mu\nu}^a(x)$, where $F_{\mu\nu}(x) = F_{\mu\nu}^a(x) T^a$. Then Eq. (2.22) still applies if all the \widehat{F} are replaced by F 's, provided $f_{\mu\alpha}^\nu(x)$ (see Eq. 2.20) is replaced by

$$f_{\mu\alpha}^\nu(x) = \int_{\mathcal{B}} \frac{d^4 p}{(2\pi)^4} \frac{e^{ipx}}{\hat{p}^2} e^{i(a_\alpha p_\alpha - p_\mu a_\mu)/2} \dot{p}_\alpha \dot{p}_\mu. \quad (2.27)$$

3. Investigating cutoff effects

In this section we investigate the numerical size of cutoff effects for two different discretization schemes of the energy momentum tensor correlators. The length of the temporal direction is set equal to $L_0 = 1/T$, where T is the temperature. There is no finite temperature at which perturbation theory correctly describes finite-volume effects, since those are related to magnetic screening, which is a non-perturbative effect. For that reason, the spatial volume is kept infinite.

We use Eq. (2.25) and perform the spatial momentum integral in Eq. (2.22) by Gaussian quadrature with a target relative accuracy of 10^{-4} . We checked a sample of the results against an extrapolation of the finite-volume momentum sums, and by comparing the latter sums to Monte-Carlo data at very high β value.

3.1 Correlators of conserved charges

We start with the isotropic lattice. Figure 1 displays the treelevel lattice correlator of the energy operator, $a_\sigma^3 \sum_{\mathbf{x}} T_{00}(x)$. The trace anomaly is formally $O(\alpha_s)$ and does not play a role at this leading order. Since in the continuum

$$C_{00,00}(x_0, \mathbf{0}) = \frac{1}{T^5} \int d^3x \langle T_{00}(x) T_{00}(0) \rangle = \frac{c_v}{T^3} \quad \forall x_0 \neq 0, \quad (3.1)$$

the departure of this correlator from a constant $c_v/T^3 = 4\pi^2 d_A/15$ is a measure of discretization errors. The discretization errors fall below the 10% level only for $x_0/a \geq 5$ for $N_\tau = 20$. The reason for this large cutoff effect is that generically $C_{\mu\nu,\rho\sigma}(x_0, \mathbf{p})$ fall off as x_0^{-5} , and this singularity must cancel in the case of $\int d^3x T_{00}(x)$. It is not surprising that this large cancellation only takes place for $x_0 \gg a$, where time-translation is effectively restored as a symmetry.

For the momentum density operator,

$$\frac{1}{3} \sum_k C_{0k,0k}(x_0, \mathbf{0}) = \frac{1}{3T^5} \sum_k \int d^3x \langle T_{0k}(x) T_{0k}(0) \rangle = \frac{s}{T^3} \quad \forall x_0 \neq 0, \quad (3.2)$$

the situation is significantly better (see Fig. 1, bottom panel), although the same cancellation has to take place. At $N_\tau = 20$, discretization errors are well below 10% for $x_0 \geq 4a$.

3.2 The tensor channel ($\xi = 1$)

In the continuum and infinite spatial volume limit, the following equality holds by rotational invariance:

$$\frac{1}{4} \int d^3x \langle (T_{11} - T_{22})(0) (T_{11} - T_{22})(x) \rangle = \int d^3x \langle T_{12}(0) T_{12}(x) \rangle, \quad \forall x_0. \quad (3.3)$$

In finite spatial volume, the two correlators differ even in the continuum. On the infinite cubic lattice, discretizing either side of Eq. 3.3 yields a correlator that approaches the continuum limit with different $O(a^2)$ discretization errors. Figure 2 shows a comparison of the discretization errors affecting these two schemes. With the clover discretization, at a given value of N_τ , discretizing T_{12} yields smaller discretization errors than discretizing $\frac{1}{2}(T_{11} - T_{22})$, for all values of x_0 .

With the plaquette discretization, Eq. 2.26, one is only able to treat the diagonal elements of $T_{\mu\nu}$, and in general it leads to significantly larger discretization errors than the clover discretization. If E refers to the chromo-electric field and B to the magnetic field, the EE and BB terms in the correlator are defined at integer values of x_0/a_τ , while the EB term is defined at half-integer values of x_0/a_τ .

For a function falling off as x_0^{-5} , without a careful treatment this mismatch leads to large $O(a^2)$ cutoff effects. An appropriate scheme [9] is to compute separately C_{BB} , C_{EE} at integer values of x_0/a and C_{EB} at half-integer values. One can then obtain the two-point function of $\frac{1}{2}(T_{11}-T_{22})$ by interpolation, which is treated as part of the treelevel improvement scheme (to be discussed in section 4). However, at treelevel, C_{EB} vanishes at the midpoint $x_0 = L_0/2$, and $C_{BB} = C_{EE}$, so it is straightforward to compare the plaquette discretization scheme to the others at that point. As figure 2 shows, its cutoff effects are almost identical to those obtained with the clover discretization of T_{12} .

In all cases, $N_\tau \geq 8$ is necessary for the cutoff effects to be less than 10% and in the $O(a^2)$ scaling region.

3.3 The scalar channel ($\xi = 1$)

We consider two ways to evaluate the zero-momentum two-point function of $\sum_k T_{kk}$ on the lattice. They differ, for large N_τ and x_0/a_τ , by $O(a^2)$ terms.

1. The first way then consists in discretizing $\sum_{i,k} C_{ii,kk}$ directly. Using the notation introduced earlier, one may rewrite it identically as

$$\sum_{i,k} \int d^3x \langle T_{ii}(0) T_{kk}(x) \rangle = \int d^3x \left(\langle \theta_{00}(0) \theta_{00}(x) \rangle - \frac{3}{2} \langle \theta(0) \theta_{00}(x) \rangle + \frac{9}{16} \langle \theta(0) \theta(x) \rangle \right). \quad (3.4)$$

2. Alternatively one can exploit the conservation of energy to write

$$\sum_{i,k} C_{ii,kk}(x_0, \mathbf{0}) = \frac{6s - c_v}{T^3} + C_{\theta\theta}(x_0, \mathbf{0}) \quad (x_0 > 0). \quad (3.5)$$

We have used the standard expressions for entropy and specific heat, $s = \frac{\partial p}{\partial T}$ and $c_v = \frac{\partial e}{\partial T}$. Here one computes the trace-anomaly correlator in a given discretization, and subtracts the thermodynamic function appearing on the right-hand side, either at the same value of N_τ or already extrapolated to the continuum.

3.3.1 Asymptotic temperatures

At high temperatures, $c_v \sim 3s$ and we have

$$\frac{6s - c_v}{T^3} = \frac{4\pi^2 d_A}{15} \left[1 - \frac{5N_c}{4} \frac{\alpha_s}{\pi} + O(\alpha_s^{\frac{3}{2}}) \right]. \quad (3.6)$$

In particular, this quantity is positive and straightforward to compute non-perturbatively. Since the θ two-point function is formally $O(\alpha_s^2)$, Eq. (3.5) implies that the leading expression for $C_{ii,kk}$ is simply Eq. (3.6), independent of x_0 . The correlators in the scalar channel thus have a large x_0 -independent contribution. At high temperatures, the choice between strategy (1.) and (2.) amounts to deciding which of $T^2(6s - c_v)$ or $\int d^3x \langle \theta_{00}(0) \theta_{00}(x) \rangle_0$ has the smaller cutoff effects. We expect the former to be the better quantity, since the latter correlator exhibits a contact term (as seen earlier), which spreads over a fixed number of lattice spacings. So provided the thermodynamic potentials are accurately known, the second strategy is the superior one.

It remains to be seen how large the cutoff effects on $\int d^3x \langle \theta(0) \theta(x) \rangle_0$ are. This is shown on Fig. 5. For $N_\tau \geq 8$, they are comparable to the cutoff effects on the T_{12} two-point function. Furthermore, they are not much larger than the cutoff effects on the entropy computed with the standard Wilson plaquette action [10], also displayed on the figure.

In summary, the trace-anomaly two-point function is computationally advantageous in that one is computing directly a quantity which is already $O(\alpha_s^2)$.

3.3.2 Temperatures close to T_c

Although perturbative methods fail near T_c , we know that very close to T_c , the specific heat c_v becomes large (both in SU(3) gauge theory and full QCD), and $6s - c_v$ is negative: it cancels a large flat contribution in the trace-anomaly correlator [11]. In that regime, it is therefore preferable to adopt the first strategy and compute $\sum_{i,k} C_{ii,kk}$ directly.

3.4 Anisotropic lattice

We now turn to the case of an anisotropic lattice, $\xi > 1$. Indeed it has long been recognized that such a lattice presents certain advantages for the calculation of thermodynamics [12] and thermal correlation functions, in particular in charmonium calculations [13].

In order to find the optimal range of anisotropies, we consider the cutoff effects on the tensor correlators at a fixed value of the spatial lattice spacing, $a_\sigma/L_0 = \text{fixed}$. We then vary the anisotropy between 1 and 4. On Fig. 3, we see that the sign of the cutoff effects changes for $1 < \xi < 2$, and goes to a finite value in the Hamiltonian limit, $\xi \rightarrow \infty$. It is clearly seen that any choice $\xi \geq 2$ reduces the cutoff effects significantly. It also appears that choosing $\xi > 3$ does not reduce the cutoff effects further, presumably because they are dominated by the coarseness of the spatial discretization. The cutoff effects appear to be minimal near $\xi = 2$, and we make the choice to investigate $\xi = 2$ in the following. In fact, as Fig. (3) shows, $N_\tau = 16$ is about as good on the $\xi = 2$ lattice as on the isotropic lattice. Because of the sign change of the cutoff effect, the smallness of the cutoff effect may be partly accidental. However, we find that other correlators are also improved. For instance, the discretization errors on the energy correlator, which are large on the isotropic lattice (Fig. 1 bottom panel), are significantly (Fig. 3) reduced at $\xi = 2$. For $N_\tau = 20$ on the anisotropic lattice, the discretization error is below 10% for $Tx_0 \geq \frac{3}{10}$, which is not the case on the $N_\tau = 10$ isotropic lattice. We remark that even in the large ξ limit, the energy correlator with the present discretization is not flat, in spite of continuous time-translation invariance being restored in that limit.

3.5 Non-zero spatial momentum

For low momenta and frequencies, hydrodynamics predicts the functional form of the spectral functions in the shear channel ($\rho_{13,13}$) and the sound channel ($\rho_{33,33}$) (see e.g. [14]). It is therefore of interest to study also correlators with non-vanishing spatial momentum [15]. An example is shown on Fig. 4 for $\mathbf{p} = (0, 0, \pi T)$. Here too the cutoff effects are smaller for the momentum density correlator than for the energy density correlator. For instance, at $N_\tau = 16$, the cutoff effects are less than 5% for $Tx_0 \geq \frac{1}{4}$ in the former case, while this level of accuracy only occurs for $Tx_0 \geq \frac{3}{8}$ in the latter case.

4. Treelevel improvement

Here we describe how the results obtained in this paper can be used to remove the dominant part of the cutoff effects on the correlators. In the case of the clover discretization, we simply divide by the treelevel lattice result, and multiply by the continuum result:

$$C_{\text{lat}}(x_0, \mathbf{p}) \rightarrow C_{\text{lat}}(x_0, \mathbf{p}) \cdot \frac{C_{\text{cont}}^{\text{t.l.}}(x_0, \mathbf{p})}{C_{\text{lat}}^{\text{t.l.}}(x_0, \mathbf{p})} \quad (4.1)$$

This technique is not new, see for instance [16].

For the plaquette discretization, the three electric-electric, magnetic-magnetic and electric-magnetic contributions to $C(x_0)$ are computed separately. For each of them, we apply the following technique [9]

to remove the tree-level discretization errors, which is adapted from static-potential studies [17]. Firstly, \bar{x}_0 is defined by the treelevel correlators such that $C_{\text{cont}}^{\text{t.l.}}(\bar{x}_0) = C_{\text{lat}}^{\text{t.l.}}(x_0)$. The improved non-perturbative correlator \bar{C} is defined at a discrete set of points through $\bar{C}(\bar{x}_0) = C(x_0)$, and then augmented to a continuous function $\bar{C} = \alpha + \gamma C_{\text{cont}}^{\text{t.l.}}$. The parameters α and γ are fixed by the condition $\bar{C}(\bar{x}_0^{(i)}) = \alpha + \gamma C_{\text{cont}}^{\text{t.l.}}(\bar{x}_0^{(i)})$, $i = 1, 2$, where $\bar{x}_0^{(1)}$ and $\bar{x}_0^{(2)}$ correspond to two adjacent measurements. The correlator is thus defined for all Euclidean times between $\bar{x}_0^{(1)}$ and $\bar{x}_0^{(2)}$. The linear combination of the electric-electric, magnetic-magnetic and electric-magnetic contributions is finally obtained at a common value of Euclidean time. Derivatives can then also be obtained from $\gamma \frac{d^n}{dx_0^n} C_{\text{cont}}^{\text{t.l.}}(x_0)$.

It is clear from this discussion that it is simpler to have a site-centered definition of the energy-momentum tensor, and this is the choice made for our large-scale calculation [4].

5. Non-perturbative study of cutoff effects

In this section we test how effective treelevel improvement is, by applying it to non-perturbative data from Monte-Carlo simulations.

5.1 Isotropic lattice, plaquette discretization

We start with data obtained on isotropic lattices with the plaquette discretization. In the scalar channel, the $C_{\theta\theta}$ correlator was obtained at several lattice spacings in [9]. Figure 5 displays the lattice spacing dependence of the $Tx_0 = \frac{1}{2}$ treelevel-improved *tensor* correlator as a function of $(aT)^2$ for two fixed temperatures. The aspect ratio of the lattice is $LT = 5$ at $1.65T_c$ and $LT = 2.5$ for $1.24T_c$. The residual discretization errors appear to be small, in fact consistent with zero for $N_\tau \geq 8$. However, a residual 10% cutoff effect cannot be excluded at $1.65T_c$, because the statistical errors are increasing with N_τ .

5.2 Anisotropic lattice ($\xi = 2$), clover discretization

Figure 5 displays the treelevel-improved correlators of the total energy and momentum on a 16×48^3 lattice. As discussed in section 3.1, these correlators are x_0 -independent in the continuum limit. In the case of the momentum T_{0k} , the correlator is flat within statistical errors down to $Tx_0 = \frac{1}{4}$ or $\frac{1}{5}$. Since this corresponds to $x_0/a_\sigma = 1.5$ and 2 respectively, we regard this as an excellent outcome. By contrast, the unimproved correlator starts to rise for x_0/a_τ larger by one unit.

In the case of the energy, the treelevel improvement imposes a much larger correction to the data, and, not surprisingly, the expected flatness of the correlator is much less well realized. The treelevel improvement undercorrects the correlator for $Tx_0 \geq \frac{1}{4}$, and overcorrects it at short distances. We have to conclude that in this channel, only the largest x_0/a_τ points are usable for a continuum extrapolation, even after treelevel improvement. In particular, this strongly restricts the x_0 -information for finite- \mathbf{p} correlators of the energy density. The latter are particularly interesting [5], because they contain information on the damping of sound waves in the plasma.

6. Concluding remarks

We have studied the discretization errors of the energy-momentum tensor correlators in lattice gauge theory. We summarize the lessons learnt.

1. using a site-centered discretization of the EMT simplifies the calculation of correlators and their treelevel improvement. Therefore in the following we discuss the ‘clover’ discretization.

2. the momentum density correlator has small cutoff effects at treelevel, and correspondingly the treelevel-improved non-perturbative correlator has small cutoff effects down to very small separations.
3. the energy density correlator is much more problematic with the chosen discretization. The treelevel energy correlator is far from being flat for realistic values of N_τ , and correspondingly after treelevel improvement cutoff effects as large as 50% remain. This implies that only the largest values of x_0 can be used in a continuum extrapolation.
4. the correlators of the spatial components of $T_{\mu\nu}$ have moderate discretization errors and treelevel improvement works well.
5. in all analyzed channels, the anisotropic lattice helps reduce the cutoff effects at a lower cost than decreasing the lattice spacing on the isotropic lattice.

The present study suggests that the design of a lattice energy density operator which leads to small cutoff effects in its two-point functions would be very valuable. Such a discretization would also have an impact in other areas of QCD, for instance in hadron structure calculations, where the glue energy density operator determines the glue momentum fraction [18, 19]. It would be interesting to investigate the cutoff effects associated with the HYP-smearred discretizations introduced in [19].

A further important issue on the anisotropic lattice is the proliferation of normalization factors that have to be applied to different components of the energy-momentum tensor. Their determination will be the subject of a separate publication.

Acknowledgments

Lattice computations for this work were partly carried out on facilities of the USQCD Collaboration, which are funded by the Office of Science of the U.S. Department of Energy, and partly on the BlueGeneL at MIT. This work was supported in part by funds provided by the U.S. Department of Energy under cooperative research agreement DE-FG02-94ER40818.

References

- [1] H. B. Meyer, *Density, short-range order and the quark-gluon plasma*, *Phys. Rev.* **D79** (2009) 011502, [[arXiv:0808.1950](#)].
- [2] H. Song and U. W. Heinz, *Extracting the QGP viscosity from RHIC data – a status report from viscous hydrodynamics*, [arXiv:0812.4274](#).
- [3] A. Nakamura and S. Sakai, *Transport coefficients of gluon plasma*, *Phys. Rev. Lett.* **94** (2005) 072305, [[hep-lat/0406009](#)].
- [4] H. B. Meyer, *Energy-momentum tensor correlators and viscosity*, *PoS LAT08* (2008) 017, [[arXiv:0809.5202](#)].
- [5] H. B. Meyer, *Energy-momentum tensor correlators and spectral functions*, *JHEP* **08** (2008) 031, [[arXiv:0806.3914](#)].
- [6] K. G. Wilson, *Confinement of quarks*, *Phys. Rev.* **D10** (1974) 2445–2459.
- [7] M. Luescher, S. Sint, R. Sommer, and P. Weisz, *Chiral symmetry and $O(a)$ improvement in lattice QCD*, *Nucl. Phys.* **B478** (1996) 365–400, [[hep-lat/9605038](#)].

- [8] H. T. Elze, K. Kajantie, and J. I. Kapusta, *Screening and Plasmon in QCD on a Finite Lattice*, *Nucl. Phys.* **B304** (1988) 832.
- [9] H. B. Meyer, *A calculation of the shear viscosity in $SU(3)$ gluodynamics*, *Phys. Rev.* **D76** (2007) 101701, [[arXiv:0704.1801](#)].
- [10] B. Beinlich, F. Karsch, and E. Laermann, *Improved Actions for QCD Thermodynamics on the Lattice*, *Nucl. Phys.* **B462** (1996) 415–436, [[hep-lat/9510031](#)].
- [11] K. Huebner, F. Karsch, and C. Pica, *Correlation functions of the energy-momentum tensor in $SU(2)$ gauge theory at finite temperature*, *Phys. Rev.* **D78** (2008) 094501, [[arXiv:0808.1127](#)].
- [12] **CP-PACS** Collaboration, Y. Namekawa *et. al.*, *Thermodynamics of $SU(3)$ gauge theory on anisotropic lattices*, *Phys. Rev.* **D64** (2001) 074507, [[hep-lat/0105012](#)].
- [13] M. Asakawa and T. Hatsuda, *J/ψ and η/c in the deconfined plasma from lattice QCD*, *Phys. Rev. Lett.* **92** (2004) 012001, [[hep-lat/0308034](#)].
- [14] D. Teaney, *Finite temperature spectral densities of momentum and R- charge correlators in $N = 4$ Yang Mills theory*, *Phys. Rev.* **D74** (2006) 045025, [[hep-ph/0602044](#)].
- [15] H. B. Meyer, *Computing the viscosity of the QGP on the lattice*, *Prog. Theor. Phys. Suppl.* **174** (2008) 220–227, [[arXiv:0805.4567](#)].
- [16] V. Gimenez *et. al.*, *Non-perturbative renormalization of lattice operators in coordinate space*, *Phys. Lett.* **B598** (2004) 227–236, [[hep-lat/0406019](#)].
- [17] R. Sommer, *A New way to set the energy scale in lattice gauge theories and its applications to the static force and alpha-s in $SU(2)$ Yang-Mills theory*, *Nucl. Phys.* **B411** (1994) 839–854, [[hep-lat/9310022](#)].
- [18] M. Goeckeler *et. al.*, *A preliminary lattice study of the glue in the nucleon*, *Nucl. Phys. Proc. Suppl.* **53** (1997) 324–326, [[hep-lat/9608017](#)].
- [19] H. B. Meyer and J. W. Negele, *Gluon contributions to the pion mass and light cone momentum fraction*, *Phys. Rev.* **D77** (2008) 037501, [[arXiv:0707.3225](#)].

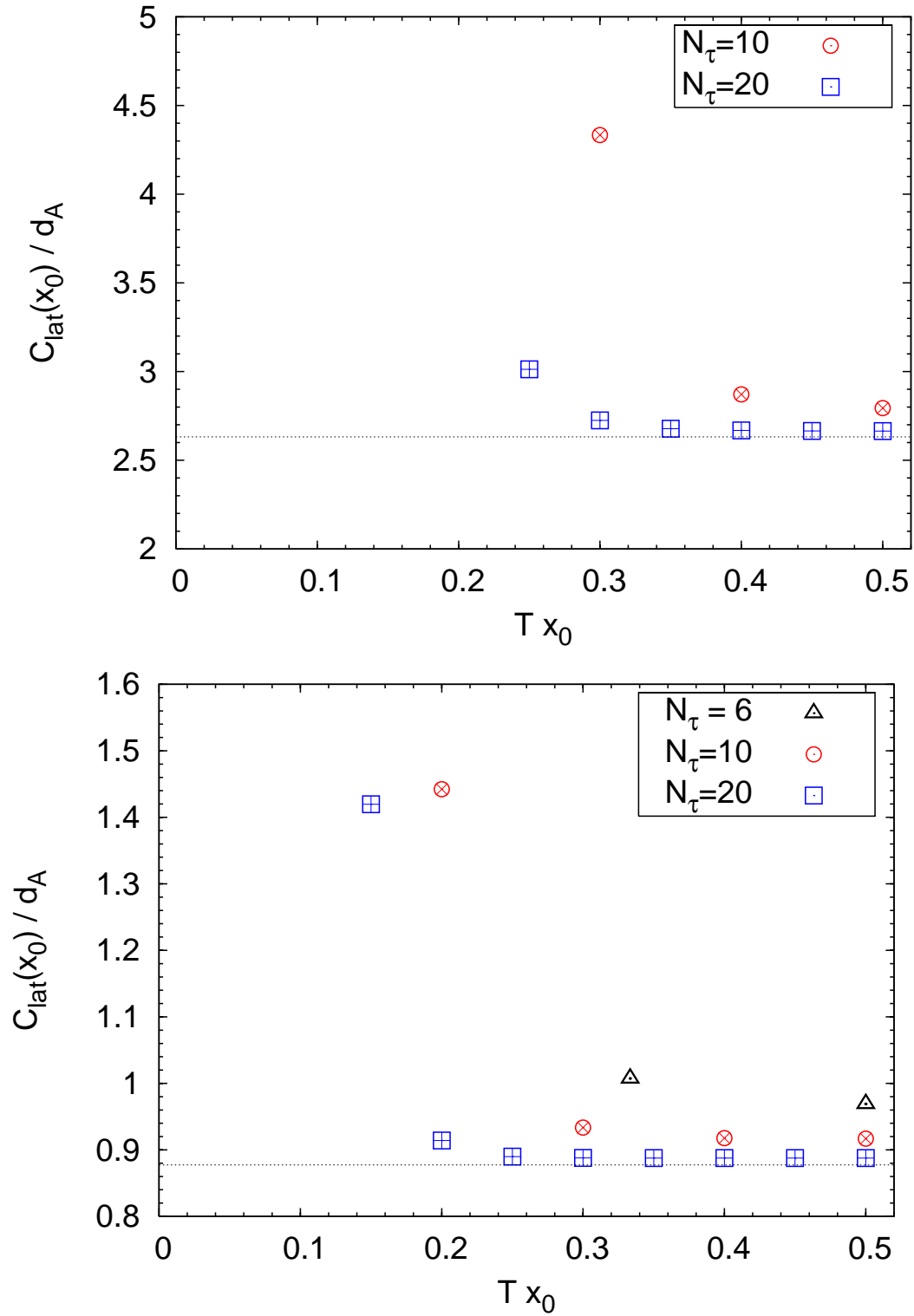


Figure 1: Top: the treelevel $C_{00,00}(x_0, \mathbf{0})$ correlator correlator at finite lattice spacing on the isotropic lattice. The horizontal line is the continuum treelevel prediction, $4\pi^2/15$. **Bottom:** the treelevel $C_{03,03}(x_0, \mathbf{0})$ correlator at finite lattice spacing on the isotropic lattice. The horizontal line is the continuum treelevel prediction, $4\pi^2/45$.

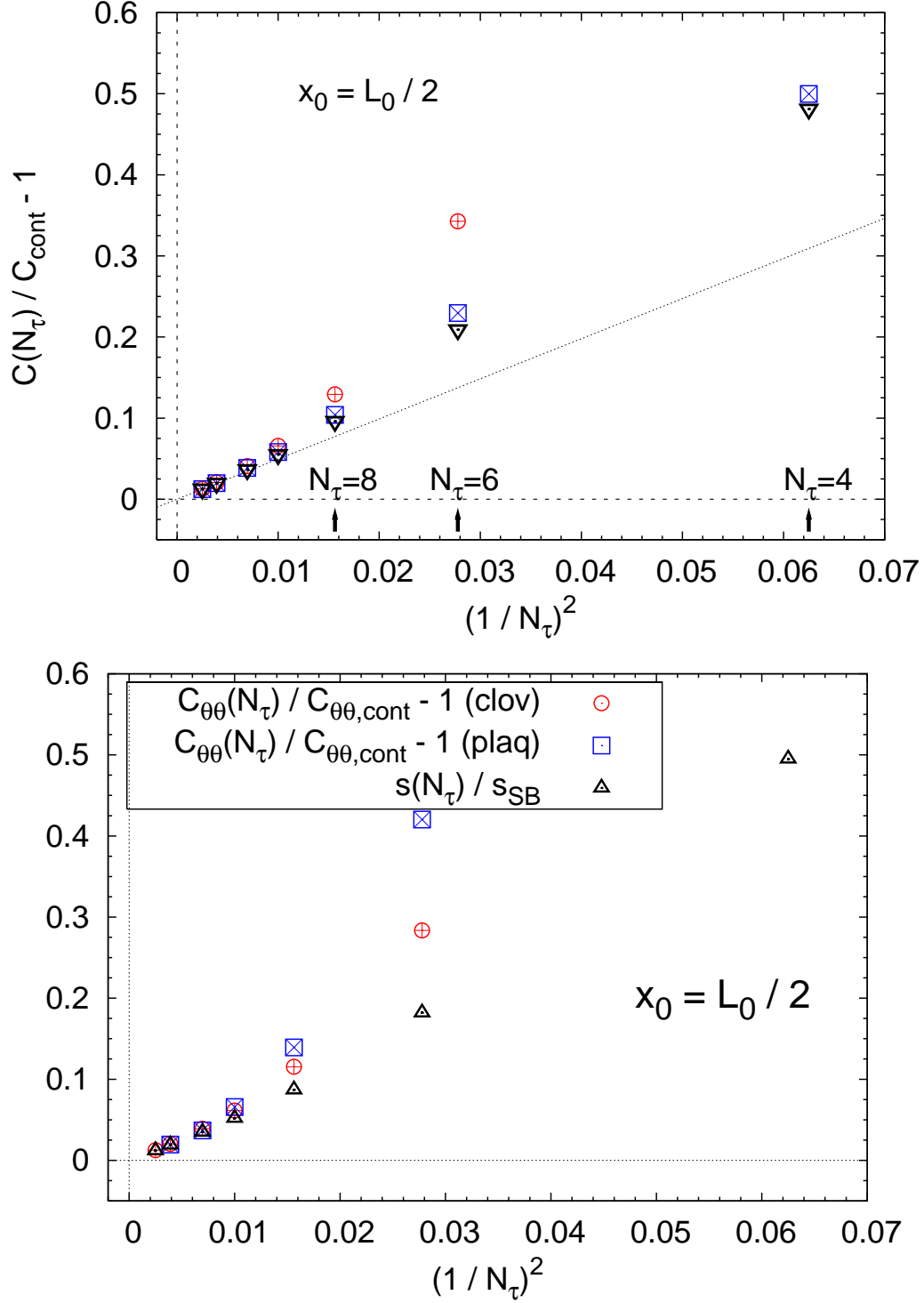


Figure 2: Top: the relative deviation of the $\mathbf{p} = 0$ tensor correlator at finite lattice spacing from the continuum correlator. The \square 's are for the clover discretization of T_{12} and the \otimes for the clover discretization of $\frac{1}{2}(T_{11} - T_{22})$. The ∇ is the plaquette discretization. **Bottom:** the cutoff effects on the $a_s^3 \sum_{\mathbf{x}} \langle \theta(0) \theta(x) \rangle_0$ correlator with the clover and plaquette discretizations. Note that $C_{\theta\theta}(N_\tau)/C_{\theta\theta,\text{cont}} = C_{00}(N_\tau)/C_{00,\text{cont}}$ at $x_0 = L_0/2$. The entropy $s(N_\tau)$ is computed with the standard Wilson action and plaquette discretization of θ_{00} [10].

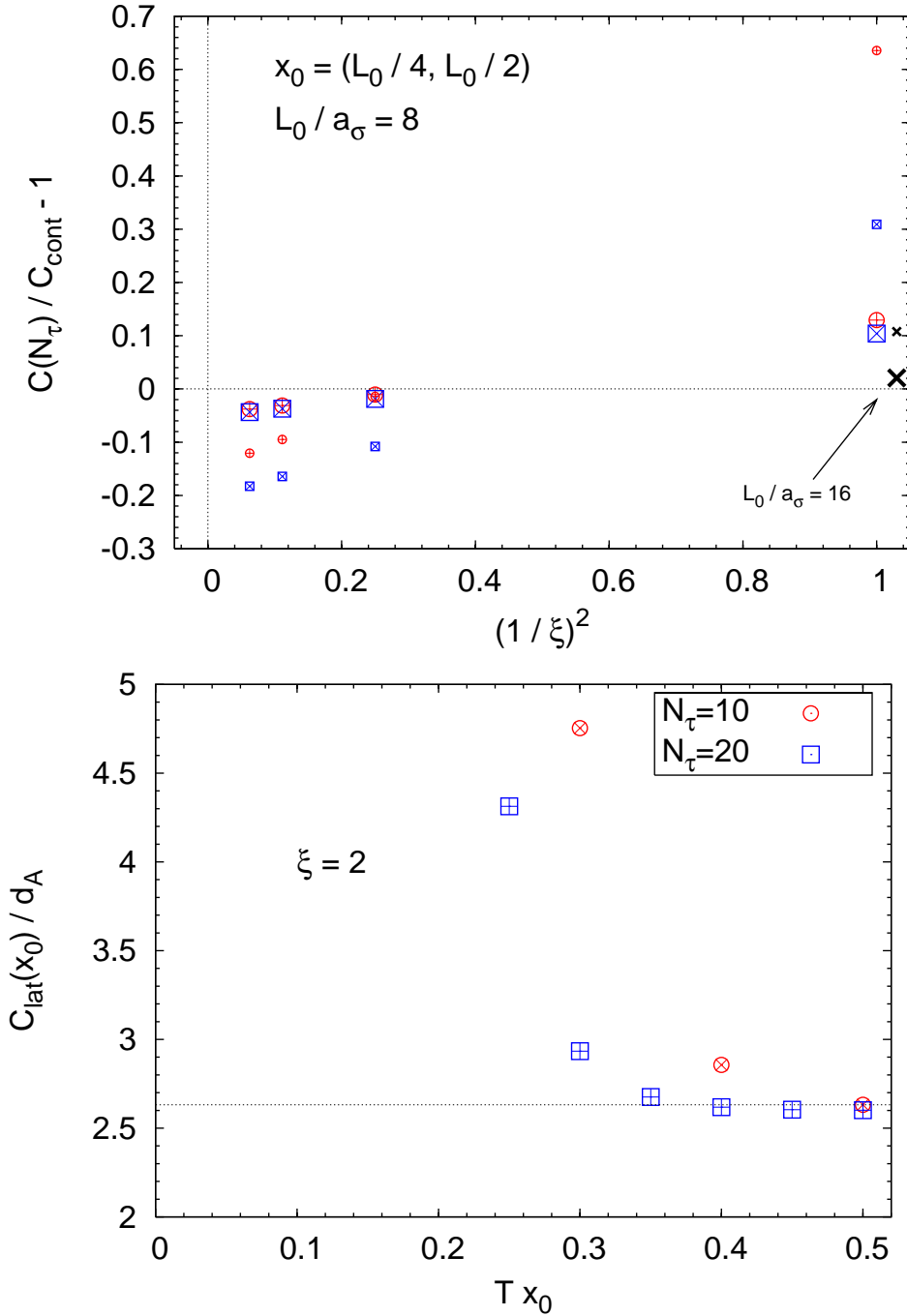


Figure 3: Top: The cutoff effects on the tensor correlator for $x_0 = L_0/4$ and $L_0/2$, corresponding to small and large symbols respectively. The spatial lattice spacing a_σ is held fixed, the temporal lattice spacing a_τ is varied between a quarter and one times a_σ . The \square 's refer to T_{12} and the \otimes 's to $\frac{1}{2}(T_{11} - T_{22})$. In addition, the two crosses at $\xi = 1$ indicate the reduction of the cutoff effect on the $\frac{1}{2}(T_{11} - T_{22})$ correlators when increasing L_0/a_σ from 8 to 16. **Bottom:** the treelevel $C_{00,00}(x_0, \mathbf{0})$ correlator on the anisotropic lattice, to be compared with Fig. (1).

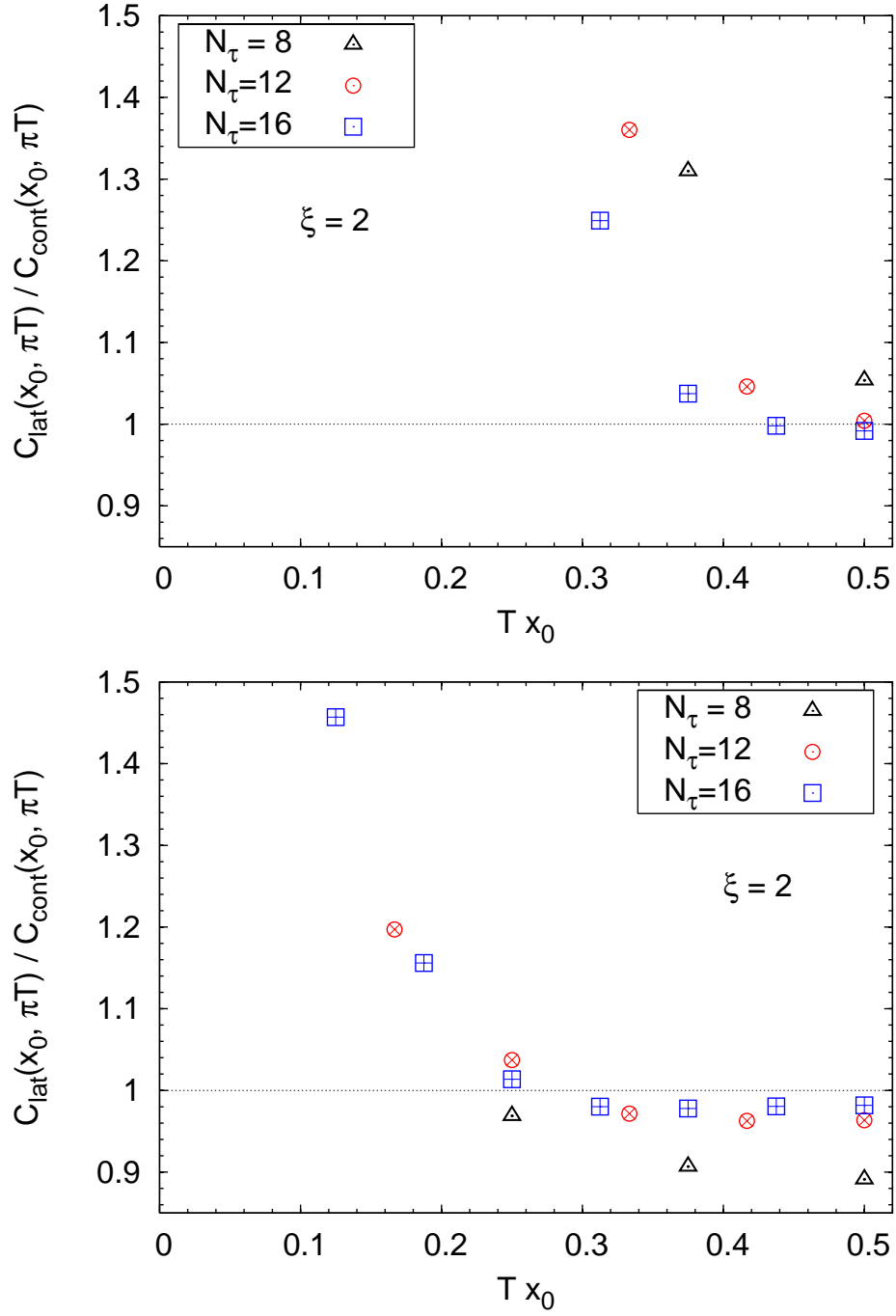


Figure 4: The ratio of lattice to continuum treelevel correlators for T_{00} (top) and T_{03} (bottom). Clover discretization on the anisotropic lattice, for $\mathbf{p} = (0, 0, \pi T)$.

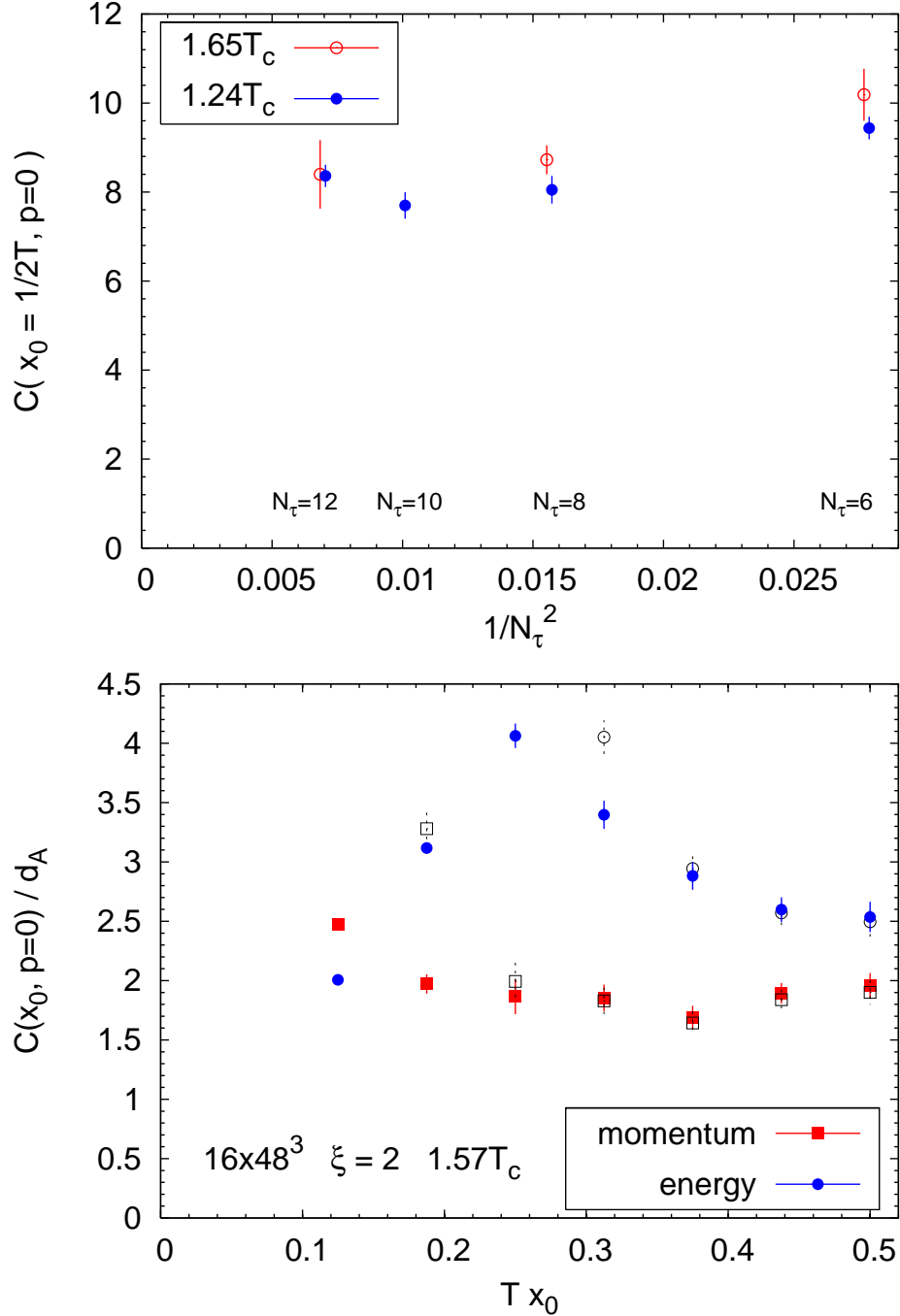


Figure 5: Top: The cutoff effects on the $\frac{1}{2}(T_{11} - T_{22})$ treelevel-improved two-point function from Monte-Carlo simulations, for two temperatures, $1.65T_c$ and $1.24T_c$. Here the plaquette discretization is used on the isotropic lattice. **Bottom:** The treelevel-improved correlators $C_{00,00}$ and $\sum_k C_{0k,0k}$ at $\mathbf{p} = 0$ calculated with the clover discretization on the anisotropic lattice at $1.57T_c$. These correlators are flat and equal to c_v and $3s$ resp. in the continuum limit. The unimproved correlators are displayed as open symbols.